

Bursting Spikes: Efficient and High-performance SNNs for Event-based Vision

Ziqing Wang^{1*}, Yuetong Fang^{1*}, Jiahang Cao¹, Renjing Xu^{1†}

Abstract—Advancing event-driven vision through spiking neural networks (SNNs) is crucial to empowering high-speed and efficient perception. While directly converting the pre-trained artificial neural networks (ANNs) - by replacing the non-linear activation with spiking neurons - can provide SNNs with good performance, the resultant SNNs typically demand long timesteps and high energy consumption to achieve their optimal performance. To address this challenge, we introduce the burst-spike mechanism inspired by the biological nervous system, allowing multiple spikes per timestep to reduce conversion errors and produce low-latency SNNs. To further bolster this enhancement, we leverage the Pareto Frontier-driven algorithm to reallocate burst-firing patterns. Moreover, to reduce energy consumption during the conversion process, we propose a sensitivity-driven spike compression technique, which automatically locates the optimal threshold ratio according to layer-specific sensitivity. Extensive experiments demonstrate our approach outperforms state-of-the-art SNN methods, showcasing superior performance and reduced energy usage across classification and object detection. Our code will be available at <https://github.com/bic-l/burst-ann2snn>.

I. INTRODUCTION

Event-driven sensing and processing have become crucial areas of research for real-time and low-latency processing. In this context, Spiking Neural Networks (SNNs) are gaining significant interest as an emerging trend in event-driven algorithms due to their inherent capability to capture spatio-temporal features of events [1], [2], [3]. SNNs consist of neurons that communicate via binary events called spikes, similar to biological neural networks. Each neuron generates a spike at each time step if its accumulated membrane potential surpasses a firing threshold, otherwise, it remains inactive. Contrasting with traditional Artificial Neural Networks (ANNs), SNNs can process information based on the timing of these spikes rather than simply relying on the activation levels of neurons alone [4]. The use of binary time series data in SNNs, as opposed to the continuous data representations in conventional networks, reduces data redundancy and lightens the processing load. When executed on neuromorphic computing devices like Loihi [5], [6] and TrueNorth [7], SNNs can achieve substantial improvements in energy efficiency. These advantages make SNNs an exciting frontier in advancing the capabilities of event-driven

devices across diverse applications from classification [8], [9], [10] to tracking [11] and image restoration [12].

While SNNs provide notable energy efficiency gains, there still remains a considerable challenge to achieving performance comparable to ANNs in real-world applications. Training SNNs from scratch is difficult because discrete spikes are non-differentiable. A well-adopted solution is gradient estimation via the differentiable surrogate gradient function. However, this approach demands massive computational resources since the computational graph grows large with multi-timestep calculations [13]. Further challenges arise from the instability in backpropagating gradients over many time steps due to the accumulation of approximation errors [14]. Another promising approach is adopting ANN-to-SNN conversion methods to convert a pre-trained ANN into SNN. Recent studies endeavor to mitigate the conversion errors by replacing the ReLU activation function in the original ANN with a crafted activation function to incorporate the dynamics of spiking neurons during fine-tuning [15], [16], [17], or calibrate the neural network parameters to align the activation between ANNs and SNNs [18]. Nevertheless, such conversion techniques fail to convert the ANNs into high-performance SNNs within an extremely limited number of timesteps. Larger timesteps contribute to increased energy costs and longer processing delays. These persisting obstacles prevent SNNs from fully realizing their practical potential for low-latency and low-power event-driven vision.

Drawing inspiration from biological nervous systems, we devise a solution that enables SNNs to have high performance, low training costs, and low latency. While most existing SNNs typically only take single spiking into account, high-frequency burst-firing neurons, which are commonly found in sensory systems, have been proven to serve distinct functions in information transmission [19], [20]. Besides, burst firing can help improve the signal-to-noise ratio of sensory responses in some systems [21], [22], [23].

Applying the burst-spike mechanism in ANN-to-SNN conversion is expected to improve the performance of the resulting SNN. Specifically, the burst-spike mechanism can increase the firing rate of postsynaptic neurons and reduce the residual information held by membrane potential after spike generation, thus facilitating information transmission and mitigating activation mismatch between ANNs and SNNs within low timesteps [24]. It has been proven that the functional implications of burst firing may differ across systems, and a similar phenomenon could occur in SNNs [25]. Our study highlights an important finding: transition losses in SNNs are not uniformly distributed across layers. Allocating

* Equal Contribution; † Corresponding Author.

¹ Ziqing Wang, Yuetong Fang, Jiahang Cao and Renjing Xu are with MICS Thrust, HKUST(GZ), Guangzhou, China, Email: wangzq37@mail2.sysu.edu.cn, yfang870@connect.hkust-gz.edu.cn, jcao248@connect.hkust-gz.edu.cn, renjingxu@ust.hk

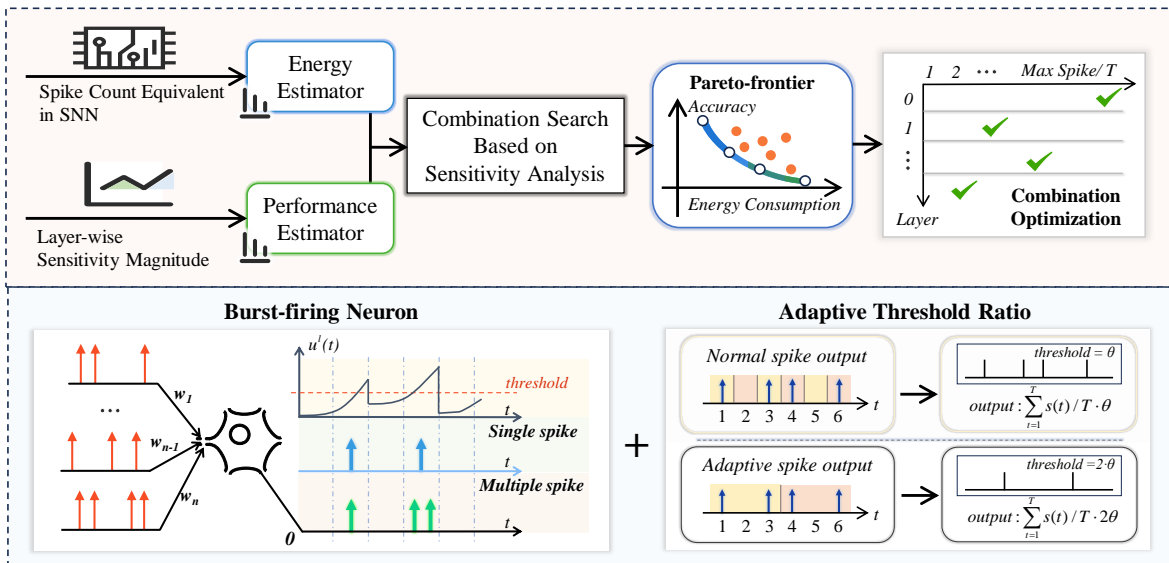


Fig. 1: **(Top)** The workflows of the Pareto Frontier-driven search algorithm to automatically search the optimal configuration of each layer in SNN. **(Bottom Left)** The concept of the burst-firing neuron, which can fire multiple spikes in one timestep. **(Bottom Right)** The concept of adaptive threshold, which can reduce the spike count with marginal information loss.

different burst-spike patterns to different layers can result in significant performance improvement and energy savings.

Contributions: In summary, the contributions of our paper are four-fold: **(I)** We introduce the burst-spike mechanism into the Spike Calibration process. Experimental results show that our method can significantly improve the accuracy at low timesteps. **(II)** We propose a Burst-Spike Reallocation (BSR) technique leveraging the Pareto frontier optimization method to automatically search for the ideal burst-spike patterns of different layers to further improve the performance under a given energy budget. **(III)** To reduce the energy during conversion, we introduce a Sensitivity Spike Compression (SSR) technique to allocate the adaptive threshold of each layer. Our results indicate a reduction in energy consumption by 30.1%, 85.2%, and 29.1% for the CIFAR10-DVS, CIFAR-10, and ImageNet datasets, respectively, with a marginal performance degradation. **(IV)** We have undertaken a thorough evaluation of our proposed framework across multiple domains, including classification, and object detection. Our findings reveal that the proposed methodology not only attains state-of-the-art performance but also a remarkable reduction in energy consumption compared to other conversion methods.

II. RELATED WORK AND PRELIMINARY

Spiking Neuron Model. For ANNs, the analogous and continuous input $\mathbf{x}^{\ell-1}$ to layer ℓ is transmitted across multiple layers by applying a linear transformation matrix \mathbf{W}^ℓ and a nonlinear activation function $f(\cdot)$, where $\ell = 1, 2, 3, \dots, L$:

$$\mathbf{x}^{\ell+1} = f(\mathbf{W}^\ell \mathbf{x}^\ell) \quad (1)$$

where the *ReLU* function is commonly adopted as $f(\cdot)$.

In SNNs, inputs are transmitted through the neuronal units, typically the Integrate-and-Fire (IF) spiking neuron in ANN-

to-SNN conversions [17], [26], [27]:

$$u^{(\ell)}(t+1) = v^{(\ell)}(t) + \mathbf{W}^{(\ell)} s^{(\ell)}(t) \quad (2)$$

$$v^{(\ell)}(t+1) = u^{(\ell)}(t+1) - s^{(\ell)}(t+1) \quad (3)$$

$$s^{(\ell)}(t+1) = \begin{cases} V_{th}^{(\ell)} & \text{if } u^{(\ell)}(t+1) \geq V_{th}^{(\ell)} \\ 0 & \text{otherwise} \end{cases} \quad (4)$$

where $u^{(\ell)}(t+1)$ denotes the membrane potential of neurons before spike generation, $v^{(\ell)}(t+1)$ denotes the membrane potential of neurons in layer ℓ at time step $t+1$, corresponding to the linear transformation matrix \mathbf{W}^ℓ , the threshold θ^ℓ , and binary output spikes $s^{(\ell)}(t+1)$ of current layer ℓ . In short, a spiking neuron is only active upon receiving or transmitting spikes, thus enabling energy-efficient processing.

ANN-to-SNN conversion and Spike Calibration. The ANN-to-SNN conversion methods [16], [17], [18], [28] involves converting a pre-trained ANN into an SNN by replacing the *ReLU* activation layers with spiking neurons. Cao et al. [29] initially exhibited that the *ReLU* neuron is functionally similar to the IF neuron. The average activation value over T timesteps in the IF neuron can be mapped onto that of the *ReLU* neuron directly. However, this method requires the timestep T must be set to infinity, or there could be considerable conversion errors.

To address this issue, Ho et al. [30], [17], [16] proposed to replace the *ReLU* activation function in the original ANN with a trainable clip function, and find the optimal data-normalization factor through a fine-tuning process to consider both accuracy and latency in the converted SNNs.

This clip function is defined as:

$$\begin{aligned}\bar{s}^{(\ell+1)} &= \text{ClipFloor}\left(W^{(\ell)}\bar{s}^{(\ell)}, T, V_{th}^{(\ell)}\right) \\ &= \frac{V_{th}^{(\ell)}}{T} \text{Clip}\left(\left[\frac{T}{V_{th}^{(\ell)}}W^{(\ell)}\bar{s}^{(\ell)}\right], 0, T\right)\end{aligned}\quad (5)$$

where $\bar{s}^{(\ell+1)}$ refers to the averaged spike output over T timesteps in converted SNNs, $\lfloor x \rfloor$ refers to the round down operator. The *Clip* function limits above but allows below, whereas the *ClipFloor* function limits a value within a range.

Although the current ANN-to-SNN method is promising, it commonly requires extensive fine-tuning epochs to obtain desired weights and thresholds, consuming a lot of computational resources. Li et al. [18] proposed activation transplanting via a layer-wise calibration algorithm aimed at diminishing the discrepancy between the original ANNs and the calibrated SNNs. This spike calibration method determines the optimal threshold by leveraging Eq. 5:

$$\min_{V_{th}} \left(\text{ClipFloor}\left(\bar{s}^{(\ell+1)}, T, V_{th}^{(\ell)}\right) - \text{ReLU}\left(\bar{s}^{(\ell+1)}\right) \right)^2 \quad (6)$$

Moreover, to align the outputs of ANN and SNN, spike calibration incorporates the expected conversion errors into the bias terms:

$$b_i^{(\ell)} := b_i^{(\ell)} + \mu_i \left(e^{(\ell+1)} \right) \quad (7)$$

where $\mu_i \left(e^{(\ell+1)} \right)$ computes the spatial mean error between the ANN and SNN outputs in the i^{th} channel.

III. METHODS

A. Spike Calibration with Burst-Spike Mechanism

With small time steps, neurons in converted SNNs generally contain substantial residual information. This is because the range of average spiking neuron output $\bar{s}^{(\ell)}$ is $[0, V_{th}^{(\ell)}]$, while the threshold from Eq. 2 is typically below the maximum activation output in ANNs. The gap in activation values between ANNs and SNNs is reflected in the residual membrane potential after spike generation. Burst-spiking neurons that fire high-frequency spikes are found in the sensory system. This distinct transmission pattern has been shown to improve the reliability of the transmission of some sensory responses [21], [22], [23]. In ANN-to-SNN conversion, introducing burst-spiking neurons can facilitate information transmission, and reduce residual information, which is expected to decrease conversion error.

We introduce the burst-spike mechanism and reconsider the dynamics of a spiking neuron to improve the spike calibration method. Different from prior studies, the burst-spike mechanism allows up to ψ spikes per timestep rather than merely one spike. This expands the range of neuronal activation output $\bar{s}^{(\ell)}$ to $[0, V_{th}^{(\ell-1)} \times \psi]$. Combining the burst-spike mechanism, the relationship of the activation output

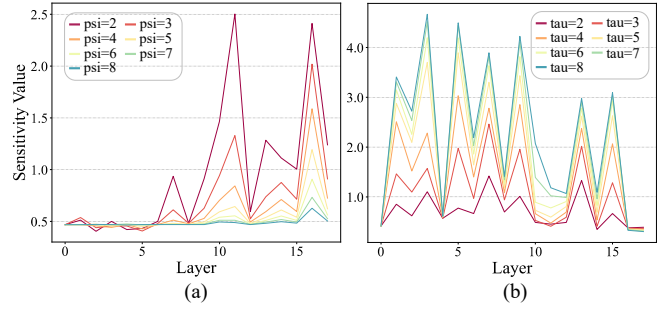


Fig. 2: **Sensitivity result of each layer in ResNet-18.** Subfigure(a): Sensitivity when using different maximum number of burst spikes ψ for each layer. Subfigure(b): Sensitivity when using different threshold ratios τ for each layer.

between ANNs and the converted SNNs then becomes:

$$\begin{aligned}\bar{s}^{(\ell+1)} &= \text{ClipFloor}\left(W^{(\ell)}\bar{s}^{(\ell)}, T, V_{th}^{(\ell)}, \psi^{(\ell)}\right) \\ &= \frac{V_{th}^{(\ell)}}{T} \text{Clip}\left(\left[\frac{T}{V_{th}^{(\ell)}}W^{(\ell)}\bar{s}^{(\ell)}\right], 0, T \times \psi\right)\end{aligned}\quad (8)$$

Correspondingly, we modify the criterion used to determine the optimal threshold as:

$$\min_{V_{th}} \left(\text{ClipFloor}\left(\bar{s}^{(\ell+1)}, T \times \psi, V_{th}^{(\ell)}\right) - \text{ReLU}\left(\bar{s}^{(\ell+1)}\right) \right)^2 \quad (9)$$

B. Burst Spike Reallocation

Biological systems, such as neurons in the human brain, exhibit unique burst-spiking patterns depending on their functions [25], [20]. Such observations inspire the optimization of artificial systems, and in the context of the ANN-to-SNN, conversion errors are found to be non-uniform across layers (Fig. 2). A straightforward solution for improving the performance is that layers with higher sensitivities to changes in ψ (maximum allowed spikes per timestep) should be allocated a larger burst-spike bound. Based on this insight, we introduce a burst spike reallocation method, taking into account both the sensitivity and energy consumption metrics.

Metrics: Sensitivity and Energy Consumption. We use Kullback-Leibler (KL) divergence as the sensitivity metric, inspired by [31]. The KL divergence measures distribution differences between ANN and SNN model outputs. Formally, the sensitivity metric for the i -th layer in terms of parameter k is defined as:

$$S_i(k) = \frac{1}{N} \sum_{j=1}^N \text{KL}\left(\mathcal{M}\left(\text{ANN}_i; x_j\right), \mathcal{M}\left(\text{SNN}_i(k); x_j\right)\right) \quad (10)$$

A smaller value of $S_i(k)$ suggests that the SNN model output remains aligned with the ANN model for the given k at layer i , indicating lower sensitivity, and vice versa. As illustrated in Fig. 2(a), early layers display a reduced sensitivity to changes in ψ , whereas deeper layers necessitate a larger ψ due to their increased sensitivity.

We measure SNN energy consumption based on the previous works [8], [17], [32]. Given that a single spike consumes

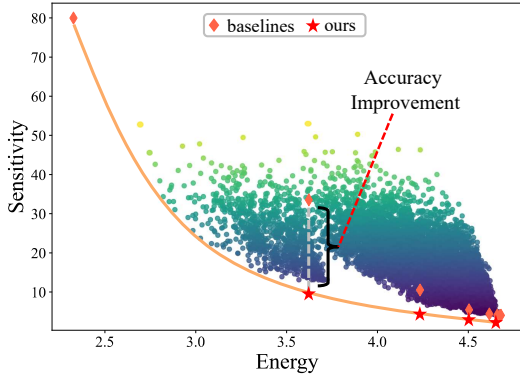


Fig. 3: **Pareto Frontier Representation.** Each data point represents a distinct layer-specific ψ configuration. The x-axis denotes estimated energy consumption for each configuration, while the y-axis displays the associated sensitivity. Given a predefined energy constraint, our Pareto frontier method can locate the optimal configuration with minimal sensitivity compared to a baseline approach without search, leading to a significant performance improvement.

α Joules and one timestep is 1 ms, energy consumption is described as:

$$E = \frac{\text{total spikes}}{1 \times 10^{-3}} \times \alpha \quad (\text{in Watts}) \quad (11)$$

Since the energy in SNN is directly tied to spike operations, we use spike count as an energy consumption indicator.

Pareto Frontier Driven Search Algorithm. Optimizing the layer-specific maximum number of burst spikes ψ is a complicated problem. For an SNN model with L layers and n configurations per layer, the possible combinations total n^L . This count grows exponentially with increasing layers.

To address the vast search space, we conduct layer-wise searches based on the dynamic programming algorithm. Our purpose is to find the optimal combination that minimizes the overall sensitivity value under a given energy threshold E_{target} , thereby improving the performance while maintaining low power consumption. The Pareto frontier method helps to identify optimal configurations eventually. The definition of the optimization problem is as follows:

$$\min_{\{k_i\}_{i=1}^L} S_{\text{sum}} = \sum_{i=1}^L S_i(k_i), \quad \sum_{i=1}^L E_i \leq E_{\text{target}} \quad (12)$$

where k_i symbolizes the chosen configuration for the i -th layer, while E_i refers to the estimated energy consumption the same layer. A fundamental assumption is the layer-wise sensitivity's independence from configurations of other layers, allowing the model's performance to be expressed as the sensitivities' sum over all layers.

By leveraging the dynamic programming algorithm, the optimal combination of ψ for various E_{target} values can be concurrently determined. As shown in Fig. 3, our method effectively balances the trade-off between energy consumption and sensitivity, achieving superior performance over baseline approaches that don't employ a systematic search strategy.

C. Sensitivity Spike Compression

High-frequency spikes in SNNs incur large energy overhead while improving the performance. We devise a method to inhibit spike generation, thereby reducing the number of spikes and energy consumption.

We optimize the total spike count according to the different firing patterns of spiking neurons. As depicted in Fig. 1, when a neuron emits spikes at regular intervals, two proximate spikes can be represented by a singular, double-amplitude spike without losing the original timing information. This process can be mathematically represented as:

$$V_{th}^{(\ell)} = \tau^{(\ell)} \cdot v_{th}^{(\ell)} \quad (13)$$

where $\tau^{(\ell)}$ refers to the threshold ratio and $v_{th}^{(\ell)}$ signifies the initial threshold of layer ℓ . The subsequent spike output of an IF neuron can be described by:

$$s^{(\ell+1)}(t) = \begin{cases} \tau^{(\ell)} \cdot V_{th}^{(\ell)} & \text{if } u^{(\ell)}(t+1) \geq \tau^{(\ell)} \cdot V_{th}^{(\ell)} \\ 0 & \text{otherwise} \end{cases} \quad (14)$$

Subsequently, the updated firing rate for SNN output is:

$$r^{(\ell+1)} = \sum_{i=1}^n W_i^{(\ell)} \frac{\sum_{t=1}^T s_i^{(\ell)}(t) \cdot \tau^{(\ell)}}{T} \quad (15)$$

Although the spike count decreases as the threshold increases, the amount of information transmitted through each neuron increases by a factor of $\tau^{(\ell)}$. Hence, the information transmitted by each layer will remain consistent.

However, optimizing spike counts is non-trivial. A naive threshold increment can lead to data loss, given the diverse firing patterns of SNN neurons. Balancing performance and energy consumption remains a challenge.

To address this, we introduce the Sensitivity Spike Compression (SSC) methodology. This method evaluates the impact of threshold changes on output fluctuations. For each layer, we strive to determine an optimal threshold ratio, denoted as τ . The goal is to reduce the spike count, ensuring minimal impact on the model's accuracy.

As illustrated in Fig. 2(b), given the sensitivities of layers to τ are different, assigning diverse τ values to each layer yields noticeable variations. An intuitive strategy is to allocate a larger τ where sensitivity is relatively small, thereby achieving a significant reduction in the overall spike count of the network. To find the desired combination, we employ the search algorithm described in Section III-B with slight modifications. The goal is modified to determine the minimum energy under a given sensitivity constraint S_{target} that corresponds to the acceptable performance degradation:

$$\min_{\{k_i\}_{i=1}^L} E_{\text{sum}} = \sum_{i=1}^L E_i(k_i), \quad \sum_{i=1}^L S_i \leq S_{\text{target}} \quad (16)$$

Empirical results have shown that the SSC approach can significantly reduce energy consumption with negligible performance loss.

TABLE I: Performance comparison between the proposed model and the state-of-the-art models on different neuromorphic datasets.

Dataset	Model	Time Steps	Accuracy (%)
CIFAR10-DVS	ANN (ResNet18)	/	82.30
	TA-SNN [38]	10	72.00
	PLIF [39]	20	74.80
	Dspkie [40]	10	75.40
	DSR [41]	10	77.30
	Spikformer [9]	10	80.90
	BS ($\psi = 8$)	8	80.41
	BS ($\psi = 8$) + BSR	8	81.25
N-Caltech101	ANN (ResNet18)	/	87.02
	SALT [42]	20	55.00
	NDA [37]	10	83.70
	BS($\psi = 8$)	8	84.69
	BS($\psi = 8$) + BSR	8	85.21
N-Cars	ANN (ResNet18)	/	97.14
	CarSNN [43]	10	86.00
	NDA [37]	10	91.90
	BS ($\psi = 8$)	8	95.93
	BS ($\psi = 8$) + BSR	8	96.24
Action Recognition	ANN (ResNet18)	/	92.22
	STCA [44]	10	71.20
	Mb-SNN [45]	10	78.10
	BS ($\psi = 8$)	8	86.88
	BS ($\psi = 8$) + BSR	8	88.21

IV. EXPERIMENT

A. Performance on Neuromorphic Dataset

Implementation Details. For neuromorphic classification tasks, extensive experimentation was conducted on a variety of neuromorphic datasets. These included CIFAR10-DVS [33], N-Caltech101 [34], N-Cars [35], and ActionRecognition [36]. Contrary to many contemporary methods that employ direct training for low latency, we opted for a conversion approach. We adopt the voxel method to convert the event into a frame, followed by integrating a reduction layer into the network [8]. We also employ data augmentation techniques [37]. For evaluating our method, we chose ResNet-18 as the backbone architecture.

Performance Comparison. As shown in Tab. I, our approach demonstrated superior performance over other leading SNN conversion techniques across the mentioned datasets within limited timesteps. Datasets like CIFAR10-DVS, N-Caltech101, and N-Cars were derived from static datasets through event-based cameras. Our results show that our approach, enhanced with Burst Spike technology, consistently outperforms other leading SNN models. For instance, our method significantly outperform the PLIF model [39], which uses 20 timesteps, by 5.6% using only 8 timesteps.

For the Action Recognition dataset, which encapsulates sequential human actions recorded with event-based cameras, our model achieve an impressive top-1 accuracy of 88.21%. This result, markedly better than alternatives, underscores our method’s adaptability to diverse neuromorphic datasets.

Furthermore, our Burst Spike Reallocation (BSR) technique proved to be instrumental in enhancing accuracy. BSR

TABLE II: Performance comparison between the proposed model and the state-of-the-art models on the ImageNet dataset.

Architecture	Method	T=8	T=16	T=32	T=64
VGG-16	OPT [28]	-	-	0.11	0.12
	SNM [46]	-	-	64.78	71.50
	QCFS [16]	-	-	68.47	72.85
	Calibration [18]	25.33	43.99	62.14	65.56
	BS($\psi = 4$)	70.03	71.98	73.61	74.18
	BS($\psi = 4$) + BSR	70.65	72.85	74.18	74.99
ResNet-34	OPT [28]	-	-	0.11	0.12
	QCFS [16]	-	-	69.37	72.35
	Calibration [18]	0.25	34.91	61.43	69.53
	BS($\psi = 4$)	69.23	72.22	74.11	74.98
	BS($\psi = 4$) + BSR	70.18	72.57	74.45	75.20

accounted for accuracy improvements of 0.84%, 0.52%, 0.31%, and 1.22% for the CIFAR10-DVS, N-Caltech101, N-Cars, and ActionRecognition datasets respectively, highlighting its efficacy.

B. Performance on Static Dataset

We extend our experimentation to the ImageNet dataset, a large-scale static dataset, to underscore the adaptability and effectiveness of our method [47]. Tab. II offers an exhaustive comparison between our method and the current state-of-the-art SNN conversion techniques. The results accentuate our method’s capability to sustain high performance, even with reduced timesteps. Typically, methods like OPT [28] and QCFS [16] exhibit accuracy reductions at fewer timesteps, as they depend on elongated timesteps to manage activation mismatch. Contrarily, our method, empowered by the Burst Spike mechanism, minimizes information loss during the conversion phase, thereby bolstering accuracy.

At comparable energy levels (specifically, $\psi = 4$), our approach, with a spike count at $T = 8$, performs on par with models set at $T = 32$. The results show that our method surpasses QCFS [16] and SNM [46] by margins of 2.18% and 5.87% respectively. Remarkably, our method exhibits a performance that’s an astounding 70.54% superior to OPT [28], underscoring our method’s superiority, particularly in limited timestep settings.

The integration of the BSR technology further augments accuracy. Specifically, BSR boosts performance by 0.95% for VGG-16 and 0.62% for ResNet-34 when operating at minimal timesteps. This phenomenon is attributed to the impact of spike distribution on accuracy during limited timesteps. By strategically reallocating spike counts to layers with heightened sensitivity, our method mitigates activation mismatch, culminating in an enriched performance.

C. Performance on Object Detection

We further evaluate our method’s potential in object detection tasks using the MSCOCO2017 dataset [50], considering its large-scale nature and inclusion of 80 object categories. Due to limited benchmarks for SNNs in object detection and the unsatisfactory results on pure event datasets, we selected

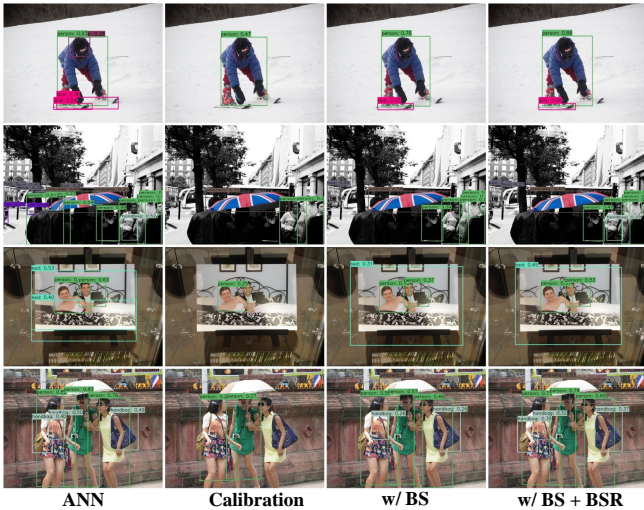


Fig. 4: Visualization of detection results on COCO.

TABLE III: Performance comparison between the proposed model and the state-of-the-art models on the COCO datasets. * represent the mAP result of ANN counterparts.

Method	Architecture	mAP*	T	mAP
Spiking-YOLO [48]	Tiny YOLO	26.24	8000	25.66
B-Spiking-YOLO [49]	Tiny YOLO	26.24	5000	25.78
Calibration [18]	YOLOv2	29.46	128	21.79
BS ($\psi = 8$)	YOLOv2	29.46	16	26.11
BS ($\psi = 8$) + BSR	YOLOv2	29.46	16	28.04

this standard dataset for our assessment. The YOLOv2 architecture with a ResNet-50 backbone served as our primary testing model, and the mean average precision (mAP) was the chosen evaluation metric.

Tab. III compare our method’s performance against established benchmarks like Spiking-YOLO [48] and its advanced variant, Bayesia-Spiking-YOLO [49]. Notably, while Spiking-YOLO attains an mAP of 26.23% with an extensive 8000 timesteps, our approach achieves a comparable mAP of 26.11% in just 16 timesteps. This represents a significant speed-up of around $500\times$ compared to Spiking-YOLO, making our method vastly more suitable for real-time applications. Further enhancing our method’s efficiency, the incorporation of the BSR technique contributes to a 1.93% improvement in mAP.

Fig. 4 provides a visualization of the results. The introduction of the BS technique markedly improves the number of objects recognized. At the same time, the introduction of the BSR technique is able to further increase the score of the recognized objects. For instance, in the first column, Calibration without the BS technique is not able to recognize the sled even with 128 timesteps. However, with the BS technique, our method is able to recognize the sled correctly using only 16 timesteps. Furthermore, contributing to the introduction of the BSR technique, the recognition of the person and the sled confidence increased from 0.76 and 0.33 to 0.88 and 0.50, respectively. This further demonstrates the effectiveness and generalizability of our proposed method.

TABLE IV: The Effectiveness of SSR Technique.

Dataset	Method	Accuracy (%)	Spike Count
CIFAR10-DVS	w/o SSC	80.41 (-0)	7.16E+09 ($\times 1$)
	w/ SSC($r=1$)	80.65 (+0.24)	5.47E+09 ($\times 0.76$)
	w/ SSC($r=1.01$)	80.30 (-0.11)	5.16E+09 ($\times 0.76$)
	w/ SSC($r=1.02$)	80.01 (-0.40)	5.00E+09 ($\times 0.69$)
CIFAR-10	w/o SSC	96.07 (-0)	8.33E+11 ($\times 1$)
	w/ SSC($r=1$)	96.03 (-0.04)	5.21E+11 ($\times 0.62$)
	w/ SSC($r=1.05$)	96.03 (-0.04)	4.74E+11 ($\times 0.57$)
	w/ SSC($r=1.10$)	95.52 (-0.55)	4.03E+11 ($\times 0.48$)
ImageNet	w/o SSC	68.04 (-0)	9.16E+13 ($\times 1$)
	w/ SSC($r=1$)	67.71 (-0.33)	7.33E+13 ($\times 0.80$)
	w/ SSC($r=1.01$)	67.36 (-0.68)	6.68E+13 ($\times 0.73$)
	w/ SSC($r=1.02$)	67.21 (-0.81)	6.57E+13 ($\times 0.71$)

TABLE V: Ablation Study of Different Techniques.

BS	BSR	SSR	Accuracy (%)	Spike Count (E+11)
			95.23 (-0.84)	8.27 ($\times 0.99$)
✓			96.07 (0)	8.33 ($\times 1$)
✓	✓		96.41 (+0.34)	2.94 ($\times 0.35$)
✓		✓	96.03 (-0.03)	4.74 ($\times 0.57$)
✓	✓	✓	96.10 (+0.03)	1.53 ($\times 0.18$)

D. Effectiveness of Sensitivity Spike Compression Technique

We apply the SSR technique to the CIFAR10-DVS, CIFAR-10, and ImageNet datasets. In Tab. V, the variable r signifies the multiplier factor of S_{target} as represented in Eq.16. By default, S_{target} is defined as the aggregate sensitivity of the model without the SSR implementation. An increased value of r provides a larger budget to cut down on spike counts, albeit potentially at the expense of performance. The empirical results highlight our method’s capability to substantially diminish spike counts with minimal trade-offs in performance. Specifically, for the CIFAR10-DVS neuromorphic dataset, assigning an r value of 1 (equating the model’s sensitivity to the baseline) yields a 23.6% reduction in spike count alongside a 0.2% accuracy improvement.

E. Ablation Study

We apply a combination of the three techniques to the CIFAR-10 dataset. It can be seen that the introduction of BS and BSR techniques can greatly improve the accuracy of SSN at low timesteps ($T = 8$), while the SSR technique is able to reduce the spike count. Furthermore, the combination of the three techniques can result in a reduction of spike count by 81.5% with 0.03% accuracy improvement.

V. CONCLUSION

In our paper, we propose a training-free ANN-to-SNN conversion framework optimized for both performance and energy efficiency. We introduce the burst spike mechanism, which significantly improves the SNN performance at low timesteps. This enhancement is further bolstered by the Burst Spike Reallocation (BSR) technique, which automates the search for the ideal burst-spike pattern for each layer. Moreover, we propose a Sensitivity Spike Compression (SSC) technique that locates the adaptive threshold to minimize energy consumption. The experimental results show that our method outperforms other conversion methods in terms of performance and energy on various vision tasks.

REFERENCES

- [1] K. Roy, A. Jaiswal, and P. Panda, "Towards spike-based machine intelligence with neuromorphic computing," *Nature*, vol. 575, no. 7784, pp. 607–617, 2019.
- [2] A. Vitale, A. Renner, C. Nauer, D. Scaramuzza, and Y. Sandamirskaya, "Event-driven vision and control for uavs on a neuromorphic chip," in *2021 IEEE International Conference on Robotics and Automation (ICRA)*. IEEE, 2021, pp. 103–109.
- [3] S. Glatz, J. Martel, R. Kreiser, N. Qiao, and Y. Sandamirskaya, "Adaptive motor control and learning in a spiking neural network realised on a mixed-signal neuromorphic processor," in *2019 International Conference on Robotics and Automation (ICRA)*. IEEE, 2019, pp. 9631–9637.
- [4] W. Maass, "Networks of spiking neurons: the third generation of neural network models," *Neural networks*, vol. 10, no. 9, pp. 1659–1671, 1997.
- [5] M. Davies, N. Srinivasa, T.-H. Lin, G. Chinya, Y. Cao, S. H. Choday, G. Dimou, P. Joshi, N. Imam, and S. Jain, "Loihi: A neuromorphic manycore processor with on-chip learning," *Ieee Micro*, vol. 38, no. 1, pp. 82–99, 2018.
- [6] M. Davies, A. Wild, G. Orchard, Y. Sandamirskaya, G. A. F. Guerra, P. Joshi, P. Plank, and S. R. Risbud, "Advancing neuromorphic computing with loihi: A survey of results and outlook," *Proceedings of the IEEE*, vol. 109, no. 5, pp. 911–934, 2021.
- [7] F. Akopyan, J. Sawada, A. Cassidy, R. Alvarez-Icaza, J. Arthur, P. Merolla, N. Imam, Y. Nakamura, P. Datta, and G.-J. Nam, "Truenorth: Design and tool flow of a 65 mw 1 million neuron programmable neurosynaptic chip," *IEEE transactions on computer-aided design of integrated circuits and systems*, vol. 34, no. 10, pp. 1537–1557, 2015.
- [8] Z. Wang, Y. Fang, J. Cao, Z. Wang, and R. Xu, "Efficient Spiking Transformer Enabled By Partial Information," Oct. 2022.
- [9] Z. Zhou, Y. Zhu, C. He, Y. Wang, S. Yan, Y. Tian, and L. Yuan, "Spikformer: When Spiking Neural Network Meets Transformer," *arXiv preprint arXiv:2209.15425*, 2022.
- [10] S. Deng, Y. Li, S. Zhang, and S. Gu, "Temporal Efficient Training of Spiking Neural Network via Gradient Re-weighting," *arXiv preprint arXiv:2202.11946*, 2022.
- [11] J. Zhang, B. Dong, H. Zhang, J. Ding, F. Heide, B. Yin, and X. Yang, "Spiking Transformers for Event-Based Single Object Tracking," in *Proceedings of the IEEE/CVF Conference on Computer Vision and Pattern Recognition*, 2022, pp. 8801–8810.
- [12] J. Cao, Z. Wang, H. Guo, H. Cheng, Q. Zhang, and R. Xu, "Spiking Denoising Diffusion Probabilistic Models," Jun. 2023.
- [13] E. O. Neftci, H. Mostafa, and F. Zenke, "Surrogate Gradient Learning in Spiking Neural Networks: Bringing the Power of Gradient-Based Optimization to Spiking Neural Networks," *IEEE Signal Processing Magazine*, vol. 36, no. 6, pp. 51–63, Nov. 2019.
- [14] W. Ponghiran and K. Roy, "Spiking neural networks with improved inherent recurrence dynamics for sequential learning," in *Proceedings of the AAAI Conference on Artificial Intelligence*, vol. 36, no. 7, 2022, pp. 8001–8008.
- [15] C. Stöckl and W. Maass, "Optimized spiking neurons can classify images with high accuracy through temporal coding with two spikes," *Nature Machine Intelligence*, vol. 3, no. 3, pp. 230–238, 2021.
- [16] T. Bu, W. Fang, J. Ding, P. Dai, Z. Yu, and T. Huang, "Optimal ANN-SNN Conversion for High-accuracy and Ultra-low-latency Spiking Neural Networks," in *International Conference on Learning Representations*, 2021.
- [17] J. Ding, Z. Yu, Y. Tian, and T. Huang, "Optimal ann-snn conversion for fast and accurate inference in deep spiking neural networks," *arXiv preprint arXiv:2105.11654*, 2021.
- [18] Y. Li, S. Deng, X. Dong, R. Gong, and S. Gu, "A free lunch from ANN: Towards efficient, accurate spiking neural networks calibration," in *International Conference on Machine Learning*. PMLR, 2021, pp. 6316–6325.
- [19] R. Krahe and F. Gabbiani, "Burst firing in sensory systems," *Nature Reviews Neuroscience*, vol. 5, no. 1, pp. 13–23, 2004.
- [20] F. Zeldenrust, W. J. Wadman, and B. Englitz, "Neural Coding With Bursts—Current State and Future Perspectives," *Frontiers in Computational Neuroscience*, vol. 12, 2018.
- [21] B. W. Connors and M. J. Gutnick, "Intrinsic firing patterns of diverse neocortical neurons," *Trends in neurosciences*, vol. 13, no. 3, pp. 99–104, 1990.
- [22] E. M. Izhikevich, N. S. Desai, E. C. Walcott, and F. C. Hoppensteadt, "Bursts as a unit of neural information: Selective communication via resonance," *Trends in neurosciences*, vol. 26, no. 3, pp. 161–167, 2003.
- [23] J. E. Lisman, "Bursts as a unit of neural information: Making unreliable synapses reliable," *Trends in neurosciences*, vol. 20, no. 1, pp. 38–43, 1997.
- [24] Y. Li and Y. Zeng, "Efficient and accurate conversion of spiking neural network with burst spikes," *arXiv preprint arXiv:2204.13271*, 2022.
- [25] Y. Mochizuki, T. Onaga, H. Shimazaki, T. Shimokawa, Y. Tsubo, R. Kimura, A. Saiki, Y. Sakai, Y. Isomura, and S. Fujisawa, "Similarity in neuronal firing regimes across mammalian species," *Journal of Neuroscience*, vol. 36, no. 21, pp. 5736–5747, 2016.
- [26] Y. Li, S. Deng, X. Dong, R. Gong, and S. Gu, "A free lunch from ANN: Towards efficient, accurate spiking neural networks calibration," in *International Conference on Machine Learning*. PMLR, 2021, pp. 6316–6325.
- [27] T. Bu, W. Fang, J. Ding, P. Dai, Z. Yu, and T. Huang, "Optimal ANN-SNN Conversion for High-accuracy and Ultra-low-latency Spiking Neural Networks," in *International Conference on Learning Representations*, 2021.
- [28] S. Deng and S. Gu, "Optimal conversion of conventional artificial neural networks to spiking neural networks," *arXiv preprint arXiv:2103.00476*, 2021.
- [29] Y. Cao, Y. Chen, and D. Khosla, "Spiking deep convolutional neural networks for energy-efficient object recognition," *International Journal of Computer Vision*, vol. 113, no. 1, pp. 54–66, 2015.
- [30] N.-D. Ho and I.-J. Chang, "TCL: An ANN-to-SNN conversion with trainable clipping layers," in *2021 58th ACM/IEEE Design Automation Conference (DAC)*. IEEE, 2021, pp. 793–798.
- [31] Y. Cai, Z. Yao, Z. Dong, A. Gholami, M. W. Mahoney, and K. Keutzer, "Zeroq: A novel zero shot quantization framework," in *Proceedings of the IEEE/CVF Conference on Computer Vision and Pattern Recognition*, 2020, pp. 13 169–13 178.
- [32] Y. Cao, Y. Chen, and D. Khosla, "Spiking deep convolutional neural networks for energy-efficient object recognition," *International Journal of Computer Vision*, vol. 113, pp. 54–66, 2015.
- [33] H. Li, H. Liu, X. Ji, G. Li, and L. Shi, "CIFAR10-DVS: An Event-Stream Dataset for Object Classification," *Frontiers in Neuroscience*, vol. 11, 2017.
- [34] G. Orchard, A. Jayawant, G. K. Cohen, and N. Thakor, "Converting Static Image Datasets to Spiking Neuromorphic Datasets Using Saccades," *Frontiers in Neuroscience*, vol. 9, 2015.
- [35] A. Sironi, M. Brambilla, N. Bourdis, X. Lagorce, and R. Benosman, "HATS: Histograms of averaged time surfaces for robust event-based object classification," in *Proceedings of the IEEE Conference on Computer Vision and Pattern Recognition*, 2018, pp. 1731–1740.
- [36] S. Miao, G. Chen, X. Ning, Y. Zi, K. Ren, Z. Bing, and A. Knoll, "Neuromorphic vision datasets for pedestrian detection, action recognition, and fall detection," *Frontiers in neurobotics*, vol. 13, p. 38, 2019.
- [37] Y. Li, Y. Kim, H. Park, T. Geller, and P. Panda, "Neuromorphic Data Augmentation for Training Spiking Neural Networks," *arXiv preprint arXiv:2203.06145*, 2022.
- [38] M. Yao, H. Gao, G. Zhao, D. Wang, Y. Lin, Z. Yang, and G. Li, "Temporal-wise attention spiking neural networks for event streams classification," in *Proceedings of the IEEE/CVF International Conference on Computer Vision*, 2021, pp. 10 221–10 230.
- [39] W. Fang, Z. Yu, Y. Chen, T. Masquelier, T. Huang, and Y. Tian, "Incorporating learnable membrane time constant to enhance learning of spiking neural networks," in *Proceedings of the IEEE/CVF International Conference on Computer Vision*, 2021, pp. 2661–2671.
- [40] Y. Li, Y. Guo, S. Zhang, S. Deng, Y. Hai, and S. Gu, "Differentiable spike: Rethinking gradient-descent for training spiking neural networks," *Advances in Neural Information Processing Systems*, vol. 34, pp. 23 426–23 439, 2021.
- [41] Q. Meng, M. Xiao, S. Yan, Y. Wang, Z. Lin, and Z.-Q. Luo, "Training High-Performance Low-Latency Spiking Neural Networks by Differentiation on Spike Representation," in *Proceedings of the IEEE/CVF Conference on Computer Vision and Pattern Recognition*, 2022, pp. 12 444–12 453.
- [42] Y. Kim and P. Panda, "Optimizing deeper spiking neural networks for dynamic vision sensing," *Neural Networks*, vol. 144, pp. 686–698, 2021.
- [43] A. Viale, A. Marchisio, M. Martina, G. Masera, and M. Shafique, "Carsnn: An efficient spiking neural network for event-based au-

- onomous cars on the loihi neuromorphic research processor,” in *2021 International Joint Conference on Neural Networks (IJCNN)*. IEEE, 2021, pp. 1–10.
- [44] P. Gu, R. Xiao, G. Pan, and H. Tang, “STCA: Spatio-Temporal Credit Assignment with Delayed Feedback in Deep Spiking Neural Networks,” in *Proceedings of the Twenty-Eighth International Joint Conference on Artificial Intelligence*. Macao, China: International Joint Conferences on Artificial Intelligence Organization, Aug. 2019, pp. 1366–1372.
- [45] Q. Liu, D. Xing, H. Tang, D. Ma, and G. Pan, “Event-based Action Recognition Using Motion Information and Spiking Neural Networks.” in *IJCAI*, 2021, pp. 1743–1749.
- [46] Y. Wang, M. Zhang, Y. Chen, and H. Qu, “Signed neuron with memory: Towards simple, accurate and high-efficient ann-snn conversion,” in *International Joint Conference on Artificial Intelligence*, 2022.
- [47] J. Deng, W. Dong, R. Socher, L.-J. Li, K. Li, and L. Fei-Fei, “Imagenet: A large-scale hierarchical image database,” in *2009 IEEE Conference on Computer Vision and Pattern Recognition*. Ieee, 2009, pp. 248–255.
- [48] S. Kim, S. Park, B. Na, and S. Yoon, “Spiking-yolo: Spiking neural network for energy-efficient object detection,” in *Proceedings of the AAAI Conference on Artificial Intelligence*, vol. 34, 2020, pp. 11 270–11 277.
- [49] S. Kim, S. Park, B. Na, J. Kim, and S. Yoon, “Towards fast and accurate object detection in bio-inspired spiking neural networks through Bayesian optimization,” *IEEE Access*, vol. 9, pp. 2633–2643, 2020.
- [50] T.-Y. Lin, M. Maire, S. Belongie, J. Hays, P. Perona, D. Ramanan, P. Dollár, and C. L. Zitnick, “Microsoft coco: Common objects in context,” in *Computer Vision–ECCV 2014: 13th European Conference, Zurich, Switzerland, September 6–12, 2014, Proceedings, Part V 13*. Springer, 2014, pp. 740–755.